Study of luminescent centers in ZnO nanorods catalytically grown on 4H-p-SiC

Nargis Bano, I Hussain, Omer Nour, Magnus Willander, P Klason and Anne Henry

Original Publication:

Nargis Bano, I Hussain, Omer Nour, Magnus Willander, P Klason and Anne Henry, Study of luminescent centers in ZnO nanorods catalytically grown on 4H-p-SiC, 2009, SEMICONDUCTOR SCIENCE AND TECHNOLOGY, (24), 12, 125015.
http://dx.doi.org/10.1088/0268-1242/24/12/125015

Study of luminescent centers in ZnO nanorods catalytically grown on 4H-p-SiC

N. Bano, I. Hussain, O. Nur and M. Willander
Department of Science and Technology, Campus Norrköping, Linköping University, SE-60174 Norrköping, Sweden
P. Klason
Department of Physics, Gothenburg University, SE-412 96 Gothenburg, Sweden
A. Henry
Department of Physics Chemistry and Biology, Linköping University, SE-58183 Linköping, Sweden

Abstract:

High quality ZnO nanorods (NRs) were grown by the vapour-liquid-solid (VLS) technique on 4H-p-SiC substrates. Heterojunction light emitting diodes (LEDs) were fabricated. Electrical characterisation including deep level transient spectroscopy (DLTS) complemented by photolumincence (PL) are used to characterize the heterojunction LEDs. On contrary to previously published results on n-ZnO thin films on p-SiC, we found that the dominant emission is originating from the ZnO NRs. Three luminescence lines have been observed, these are associated with blue (465 nm) and violet (446 nm) emission lines from ZnO NRs emitted by direct transition/recombination of carriers from the conduction band to a zinc vacancy (V_{Zn}) radiative centre and from zinc interstitial (Zn_i) radiative center to the valance band. The third green-yellow (575 nm) spectral line is emitted due to a transition of carriers from Zn_i to V_{Zn}. The superposition of these lines led to the observation of strong white light which appears as a wide band in the room temperature PL.

PACS: 85.60.Jb, 61.46.Km, 71.55.-i, 71.55.Gs

1. Introduction

Oxide semiconductors have been viewed as highly promising materials for future electronic devices; compared to other oxide semiconductors ZnO has a large direct band gap (3.3 eV) with high exciton binding energy (60 meV) which can provide more efficient excitonic emission even above room temperature. In addition ZnO is a very good candidate for light emitting diode (LEDs) due to emissions in the visible region by intrinsic/extrinsic defects and has a significant advantage for ultraviolet (UV) lasing applications [1]. However, the difficulty of ZnO p-type doping impedes the fabrication of a ZnO homostructural diode but the growth of n-type ZnO on other p-type materials could provide an alternative way to realize ZnO-based p-n heterojunctions [2]. The main factor which influences the properties of the p-n heterojunctions is the close lattice match of the ZnO layer and the substrate employed. 4H-SiC is a good candidate for the growth of n-ZnO, since 4H-SiC has the same wurtzite crystalline structure and relatively small lattice mismatching to ZnO (~5%) [3]. But despite this, there have been only a few reports on the growth of n-type ZnO thin film on p-type SiC. H. Morkoç et. al. [4] fabricated a n-ZnO/p-SiC type heterojunction diode by using unintentionally n-type doped ZnO thin films grown on top of a low temperature ZnO buffer layer on p-type SiC substrates by plasma-assisted molecular-beam epitaxy (MBE). They measured the electro-optical properties. Their data indicated that mainly electron injection from the ZnO side of the heterojunction into p-SiC side takes place. As a result, the emission properties of n-ZnO/p-SiC diodes were determined by the luminescence properties of p-SiC and indicated a high density of interface states.

On the other hand ZnO nanostructures such as nanorods (NRs) have attracted considerable attention owing to their large surface area, good crystal quality, unique photonic properties. ZnO has a rich family of nanostructures that can easily be grown even on very cheap substrates such as glass and plastic [5, 6]. The reason for this is that the nanorods can release the strain/stress due to substrate mismatch through relatively large surface area. ZnO has two main emission bands in its room temperature (RT) photoluminescence (PL) spectrum, these are a sharp UV band and a broad emission band, lies between 420 to 700 nm. The later is called deep band emission and historically denoted as the green band emission [2, 7]. Many different models have been proposed to explain the nature of the deep band emission. The deep band emission in ZnO is suggested to be a result of a superposition of different PL bands [2]. The origin of this deep band emission is still under discussion. ZnO can exhibit different emissions in the visible range including violet, blue, green, yellow, and orange-red which are associated with intrinsic as well as extrinsic defects in the material [8, 9]. In general defects in ZnO thin film have been extensively investigated by a variety of experimental techniques e.g., electron paramagnetic resonance EPR, cathode luminescence, positron annihilation spectroscopy, perturbed angular correlation spectroscopy and deep-level transient spectroscopy DLTS. However, there still exist controversies on the origin of defect species that dominates the emission properties of ZnO, and the unambiguous electron transition pathways are unknown yet in detail [10, 11]. Particularly for the violet, blue and green-yellow emissions in ZnO, there are only very limited reports.

In this study we report on the violet, blue and green-yellow emission luminescence centers in ZnO nanorods grown on p-SiC. The violet, blue and green-

yellow emission luminescence lies in the deep band emission (420-700 nm) which is a result of superposition of different defect bands emitting in different wavelengths. During experiments we observed strong white light which is evidence that this emission is a superposition due to different defects in ZnO NRs. We have used electrical characteristics and deep-level transient spectroscopy (DLTS) complemented by photolumincence (PL) to display and analyze the luminescence characteristics.

2. Experimental details

ZnO NRs were grown on 4H-p-SiC thin layer with acceptor concentration around $5x10^{18}$ cm^{-3} by chemical vapour deposition on n-SiC commercial substrate [12]. We adopted the vapour-liquid-solid (VLS) technique for the growth of ZnO NRs [13]. First we cover small portion of the p-SiC substrate for ohmic contact on p-SiC after that a layer of Au nano-particles were deposited on the SiC substrate. ZnO(99.9%) powder was mixed with graphite (99.9%) powder with 1:1 ratio, then the mixed powder was vaporized. The substrate coated with Au is placed within a certain distance from a boat containing the mixture of ZnO and graphite powder and then grown at 890 ^{0}C for 30 min.

The device structure was characterized by scanning electron microscope (SEM). The samples were also characterized with photoluminescence (PL) at RT. The laser lines with wavelength of 270 nm or 350 nm from an Ar^+ laser were used as the excitation sources.

After growth the samples were used to process light emitting diodes (LEDs). For the ohmic contact on 4H-p-SiC we first etch a small portion of SiC which we cover before the growth of ZnO NRs after that a thin layer of Ni\Al was used. The contact was

annealed at 900 ^{o}C for 3 min in Ar atmosphere. Prior the ohmic contacts on the ZnO NRs an insulating PMMA layer was deposited between the NRs. To ensure that no PMMA was on the top of the NRs oxygen plasma cleaning was performed prior to the contact metal deposition. Then Al contacts of diameter 0.5 mm were evaporated onto a group of NRs.

Current-voltage (I-V) characteristics for ZnO nanorods on p-4H-SiC were also perform to see current transport mechanism. To determine the doping concentration, built-in-voltage and the defects in ZnO nanorod additional electrical measurements were also performed by using C-V and DLTS.

3. Results and discussion

Figure 1 shows an equilibrium energy band diagram of p-n heterojunction of p-4H-SiC and n-ZnO. Here the bandgap (Eg) of ZnO is 3.3 eV and that of 4H-SiC is 3.23 eV. The conduction band offset (ΔE_C) for electrons is $\Delta E_C = \chi_{ZnO} - \chi_{SiC} = 0.3$ eV, where χ is the electron affinity. While the valance band offset (ΔE_V) for holes is ΔE_V = Eg (ZnO) $+\Delta E_C -$ Eg (SiC) = 0.4 eV. ΔE_V has a higher value than ΔE_C, which means that electron injection from n-ZnO to p-SiC is larger than hole injection from p-SiC to n-ZnO [14, 15].

The device structure was characterized by scanning electron microscope (SEM). The ZnO NRs were grown vertically aligned (length 1.9-2.2 μm and width 0.4-0.6 μm) as shown in the SEM image in Figure 2.

Figure 3 represents a typical current-voltage (I-V) characteristic for ZnO nanorods/p-SiC heterojunction at room temperature (RT). The value of the ideality factor

was obtained from the slope of linear region of semi-logarithmic I-V plots. The ideality factor was found to be in the range 3-4 for all diodes investigated. The higher value of the ideality factor indicates that the transport mechanism is no longer dominated by the thermionic emission [16]. Nonideal behavior is often attributed to defect states in the band gap of the semiconductor or at the interface providing other current transport mechanisms such as structural defects, surface contamination, barrier tunneling or generation recombination in the space charge region and to variations in interface composition [16]. To understand which mechanisms can control the junction behavior, the I-V characteristics of the device is studied in log-log scale.

The log-log plot of the I-V data at RT is shown in Fig. 3 (inset) and it illustrates the current transport mechanism exhibit in a three different regions. The current in region I follow a linear dependence, i.e. I~V. This indicates the current transport is dominated by tunneling at low voltages. The boundary for this region was determined to be below 0.03 V. In region II (0.04-1 V) the current increases exponentially as a relation of I~ exp (cV) where c=q/nkT. The ideality factor (3-4) is determined in this region and the dominating transport mechanism is recombination-tunneling. Finally above 1 V the current follows a power law ($I \sim V^2$), indicating a space-charge limited current transport mechanism. Space charge limited current (SCLC) and at least one of the other regions observed in the present study have been reported different n-ZnO nanorods/p-Si heterojunctions [17, 18] and in Schottky contact to ZnO nanorods [19].

Additional electrical measurements were also perform using C-V and a typical C-V measurement at room temperature of the heterojunction LED is shown in Figure 4. Depth profile shows that the non-uniform behavior which is an evidence of traps in the

sample (inset Fig. 4). The doping concentration and the built-in-voltage were determined from the slop and intercept of $1/C^2$ versus V plots and were found to be $1.4\times10^{18}cm^{-3}$ and 1.4 V respectively.

The associated DLTS spectra of ZnO under identical conditions: (V_P/V_R = 0/-5, t_p = 20 µs, rate window 4550 s^{-1}) is shown in Figure 5 (a). This DLTS spectrum shows two levels, one electron trap and one hole trap labeled as E1 and P1 respectively. The activation energies and capture cross-sections of these levels are calculated by using D. V. Lang's line shape formula [20]. The levels E1 and P1 yielded activation energies (capture cross sections) as 0.52 eV (2.7×10^{-15} cm^2) and 0.635 eV (2×10^{-14} cm^2), respectively. The trap concentration (N_t) for the E1 and P1 are found to be 1×10^{15} cm^{-3} and 7×10^{14} cm^{-3}, respectively. The traps observed in our ZnO NRs are of great interest because of the fact that the defect-induced electronic states in the band gap can significantly alter the optical performance of the device under operation.

Several groups have reported that different defect centers in ZnO are responsible for blue, green, yellow, and red emissions [21, 22], the green emission is associated with oxygen vacancy, orange-red emission is associated with excess oxygen [23], red emission is attributed to the interstitial zinc (Zn_i) [21]. Recently it was reported that the violet emission corresponds to Zn_i and transition involving V_{Zn} would result in a blue emission [22-24]. It is reported that in wide band gap semiconductors the broad band luminescence is related to the transitions from donor states to the deep acceptor states [25].

Based on these evidences, we have correlated E1 and P1 traps as radiative centers for the carriers to emit blue, violet and green-yellow in the probable emission spectra. For this purpose, we have used simple energy–wavelength relation: $E = hc/\lambda$, calculated the

wavelength and in this way identified the components in the emission spectrum. Here E is the activation energy of the level with respect to the conduction band edge. As a result, blue (465 nm) and violet (446 nm) spectral lines are found to be emitted by direct transition/recombination of carriers from the conduction band to the radiative centre V_{Zn} (P1) and from radiative center Zn_i (E1) to valance band. Moreover green-yellow (575 nm) spectral line is found to be emitted by transition of carriers from traps Zn_i to V_{Zn}. The UV spectral line (380 nm) would appear due to direct transition/recombination between conduction bands to the valence band. The detail of this emission model is illustrated in the Fig. 5(b); we have skipped band bending and transitions via shallow levels, for the sake of convenience.

Similarly, evidence supporting the argument comes from our RT-PL spectra of ZnO nanorods. Figure 6 consisted of an intense narrow ultraviolet (UV) centered at around 380nm and a defect related wide band (420-700 nm). It is extensively reported that this broad deep band emission is a defect related emission and that it is a superposition of different defect bands emitting in different wavelengths [2, 8, 26]. This is probably one reason for the debate, since different samples have different defect configuration due to different growth methods and growth conditions. The peak position of the deep band emission is defined according to the relative density of these radiative defects. The radiative defects observed here lies within the deep band emission (420-700 nm) of Fig. 6. The origin of blue (465 nm) and violet (446 nm) spectral lines are documented to be due to V_{Zn} and Zn_i respectively [22-24]. Examples of some of the reported radiative defects within the deep band emission are reported in different studies, Leiter et. al. observed a broad, green band centered at 2.45 eV and assigned it to the

oxygen vacancy (Vo) [27]. Some other groups have attributed the deep band emission to Vo [28-30]. Using theoretical considerations, the 2.38 eV green emissions observed by PL has been attributed to the oxygen antisite (O_{Zn}) [31]. Other candidates are the Zn vacancy (V_{Zn}) [8, 32, 33], interstitial zinc (Zn_i), as well as extrinsic impurities such as copper [29,34]. T. Moe. Børseth et. al. [26] recently reported that the Vo, and V_{Zn} defects are responsible for the deep band emission and V_{Zn}-related defects are present at an energy level equal to 2.53 eV. This implies that our P1 level located at E_c - 2.66eV may be related to V_{Zn}. Recently it was reported that the violet emission from undoped ZnO corresponds to Zn_i [22]. Lin and coworkers have calculated the transition energy from Zn_i level to the valance band 2.9 eV [35]. This approximate agrees well with our experimental results, the transition energy from the observed Zn_i to valance band is 2.8±0.02 eV.

Results from previously published heterojunction LED based on ZnO thin films, grown on SiC by plasma-assisted molecular-beam epitaxy showed that only an emission from SiC was observed [2, 4]. This was a consequence of the high density of interface states. To the contrary, as our present results showed, we have the different situation. The different result obtained here is justified by the much better interface at the pn hetrojunction. This is because the lattice mismatch difference and the associated stress/strain in the case of ZnO nanorods are released through the large surface area of the nanorods. Adding to that nanorods have a small foot prints and hence is easier to grown with compare to the thin films. Hence a better pn hetrojunction interface and a better ZnO quality is achieved in the case of NRs compared ZnO thin film grown on SiC substrate [2, 4].

4. Summary

In summary, electrical and optical properties of n-ZnO nanorods grown on 4H-p-SiC by vapour-liquid-solid (VLS) method have been studied. The I-V curve exhibited nonlinear and good rectifying behavior and through C-V measurement we extracted the doping concentration in the ZnO nanorods to be $1.4\times10^{18}cm^{-3}$. C-V and DLTS shows the presence of two traps labeled as E1 and P1 with activation energies (capture cross sections) of 0.52 eV (2.7×10^{-15} cm^2) and 0.635 eV (2×10^{-14} cm^2) and trap concentration (N_t) 1×10^{15} cm^{-3} and 7×10^{14} cm^{-3}, respectively. We correlate E1 trap with zinc interstitial (Zn_i) and P1 trap with zinc vacancy (V_{Zn}) related defects. We have correlated traps as radiative centers for the carriers to emit violet (446 nm), blue (465 nm) and green-yellow (575 nm) light.

Acknowledgments

The financial support from the NANDOS EU project is appreciated.

References:-

[1] Wei Z P, Lu Y M, Shen D Z, Zhang Z Z, Yao B, Li B H, Zhang J Y, Zhao D X, Fan X W and Tang Z K 2007 *Appl. Phys. Lett*. **90** 042113.

[2] Özgur U, Alivov Ya I, Liu C, Teke A, Reshchikov M, Dogan S, Avrutin V, S. -J. Cho S -J and Morkoç H 2005 *J. Appl. Phys*. **98** 041301.

[3] Clement Yuen, Yu S F, Lau S P, Rusli and Chen T P 2005 *Appl. Phys. Lett*. **86** 241111.

[4] Alivov Ya I, Johnstone D, Özhur U, Avrutin V, Fan Q, Akarca-Biyikli S S and Morkoç H 2005 *J. Appl. Phys*. **44** 7281.

[5] Jagadish C and Pearton S J 2006 Zinc Oxide Bulk, Thin Films and Nanostructures, Elseviser Ltd.

[6] Wadeasa A, Nur O and Willander M 2009 *Nanotechnology*. **20** 065710.

[7] Zhao Q X, Klason P. Willander M, Zhong H M, Lu W and Yang J H 2005 *Appl. Phys. Lett.* **87** 211912.

[8] Klason P, Børseth T M, Zhao Q X, Svensson B G, Kuznetsov A Y, Bergman P J and Willander M 2008 *Solid State Communications* **145** 321.

[9] Klingshirn C 2007 *Phys. stat. sol.* **244** 3027.

[10] Vanheusden K, Seager C H, Warren W L, Tallant D R and Voigt J A 1996 *Appl. Phys. Lett.* **68** 403.

[11] Ohashi N, Nakata T, Sekiguchi T, Hosono H, Mizuguchi M, Tsurumi T, Tanaka J, and H. Haneda H 1999 *Jpn. J. Appl. Phys. Part 2* **38** L113.

[12] Henry A, Hassan J, Bergman J P, Hallin C, Janzen E 2006 Chem. *Vap. Deposition* **2** 475-482.

[13] Klason P 2008 *Ph.D. Thesis*, Department of Physics, University of Gothenburg, ISBN 978-91-628-7492-6.

[14] Aranovich J A, Golmyo D, Fahrebruch A L and Bube R H 1980 *J. Appl. Phys.* **51** 4260.

[15] El-Shaer A, Bakin A, Schlenker E, Mofor A C, Wagner G, Reshanov S A and Waag A 2007 *Superlattices and Microstructures.* **42** 387.

[16] Allen M W and Durbin S M 2008 *Appl. Phys. Lett*. **92** 12110.

[17] Chen X D, Ling C C, Fung S, Beling C D, Mei Y F, Ricky K. Y. Fu, Siu G G, and Paul. K. Chu 2006 *Appl. Phys. Lett*. **88** 132104.

[18] Koteeswara Reddy N, Ahsanulhaq Q, Kim J H, and Hahn Y B 2008 *Appl. Phys. Lett*. **92** 043127.

[19] Klason P, Nur O, and Willander M 2008 *Nanotechnology* **19** 475202.

[20] Lang D V 1974 *J. Appl. Phys*. **45** 3023.

[21] Djurisc A B, Leung Y H, Tam K H, Ding L, Ge W K, Chen H Y, Gwo S 2006 *Appl. Phys. Lett*. **88** 103107.

[22] Ahn C H, Kim Y Yi, D. C. Kim D C, Mohanta S K, and Cho H K 2009 *J. Appl. Phys*. **105** 13502.

[23] Xu P S, Sun Y M, Shi C S, Xu F Q, Pan H B 2003 *Nucl. Instrum. Methods B* **199** 286.

[24] Tam K H, Cheung C K, Leung Y H, Djurisic A B, Ling C C, Beling C D, Fung S, Kwok W M, Chan W K, Phillips D L, Ding L and Ge W K 2006 *J. Phys. Chem. B* **110** 20865.

[25] Mattila J, Nieminen R M 1997 *Phys. Rev. B* **55** 9571.

[26] Børseth T M, Klason P, Zhao Q X, Willander M, Svensson B G and Kuznetsov A Y 2006 *Appl. Phys. Lett*. **89** 262112.

[27] Leiter F H, Alves H, Pfisterer D, Romanov N G, Hofmann D M, and Meyer B K 2003 *Physica B* **340–342**, 201.

[28] Vanheusden K, Seager C H, Warren W L, Tallant D R, and Voigt J A 1995 *Appl. Phys. Lett*. **68** 403.

[29} Jeong S -H, Kim B -S, and Lee B -T 2003 *Appl. Phys. Lett*. **82** 2625.

[30] Shan F K, Liu G X, Lee W J, Lee G H, Kim I S, and Shin B C 2005 *Appl. Phys. Lett*. **86** 221910.

[31] Lin B, Fu Z, and Jia Y 2001 *Appl. Phys. Lett*. **79** 943.

[32] Kohan A F, Ceder G, Morgan D, and Van de Walle C G 2000 *Phys. Rev. B* **161** 15019.

[33] Janotti A and Van de Walle C G 2006 *J. Cryst. Growth* **287** 58.

[34] Garces N Y, Wang L, Bai L, Giles N C, Halliburton L E, and Cantwell G 2002 *Appl. Phys. Lett*. **81** 622.

[35] Lin B X, Fu Z X, and Jia Y B 2001 *Appl. Phys. Lett*. **79** 943.

Figure captions

Figure 1: Shows a typical fabricated band diagram of p-n hetero junction of 4H-p-SiC and n-ZnO.

Figure 2: SEM image of ZnO NRs grown on 4H-SiC substrate before spin coating and inset shows after spin coating and baking

Figure 3: Typical Current-voltage characteristics for ZnO NRs and in inset the log-log current-voltage data for ZnO NRs .

Figure 4: Typical C-V characteristics of n-ZnO nanorods/p-SiC heterojunction LED measured at room temperature and inset shows the depth profile.

Figure 5: (a) Representative DLTS spectra of ZnO NRs. Filled circles (experimental) and solid line (line shape fit) which shows two traps E1 (electron trap) and P1 (hole trap). (b) Schematic band diagram the three observed luminescence process.

Figure 6: PL spectrum for ZnO NRs measured using an Ar- laser operating at 150 mW at room temperature.

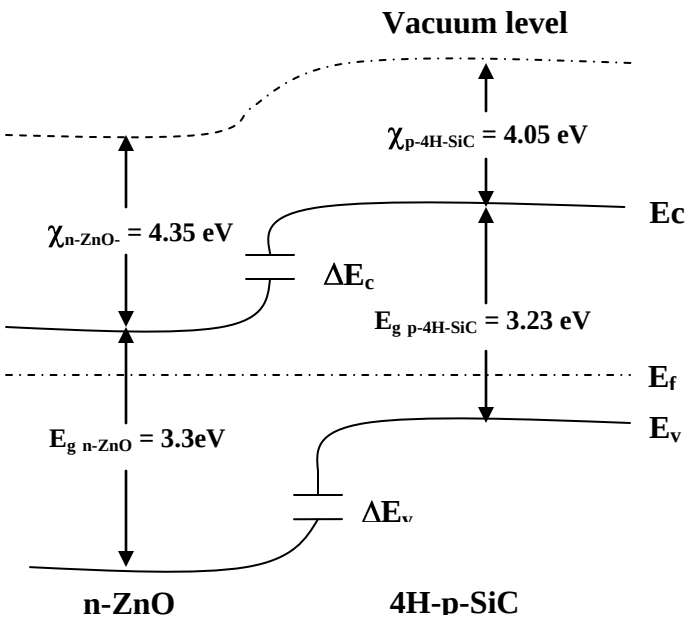
Vacuum level
χp-4H-SiC = 4.05 eV
Ec
χn-ZnO- = 4.35 eV
ΔEc
Eg p-4H-SiC = 3.23 eV
Ef
Ev
Eg n-ZnO = 3.3eV
ΔEv
n-ZnO
4H-p-SiC

Figure 1

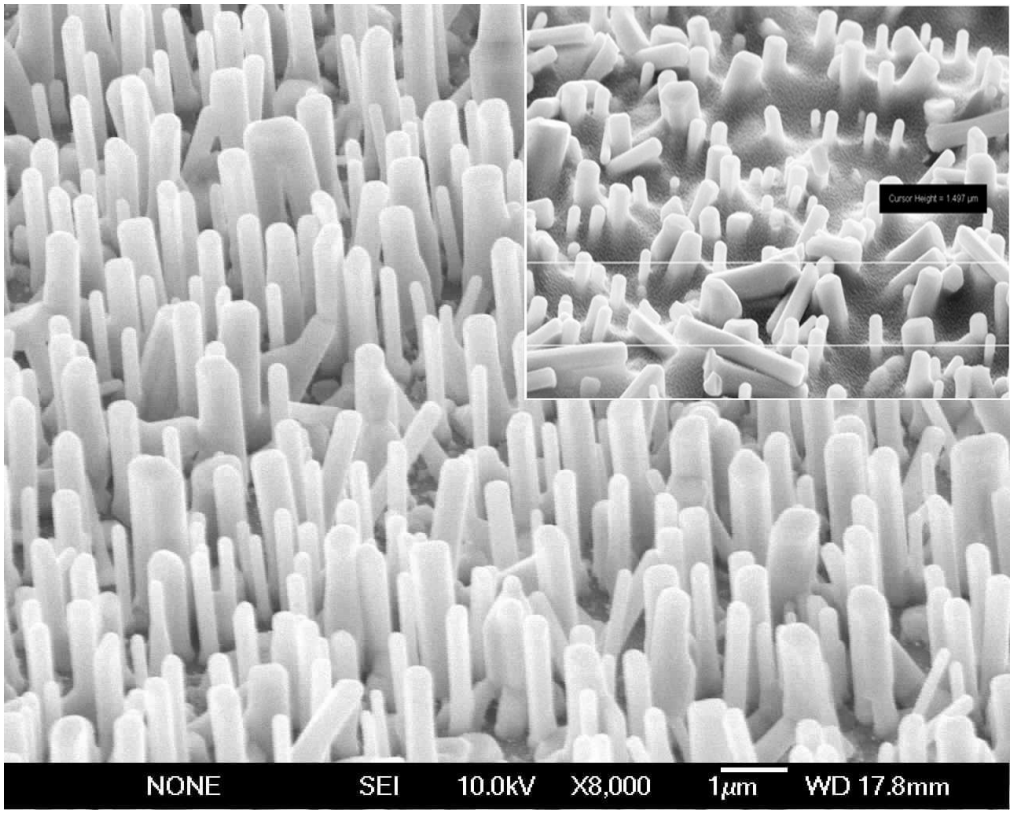

Figure 2

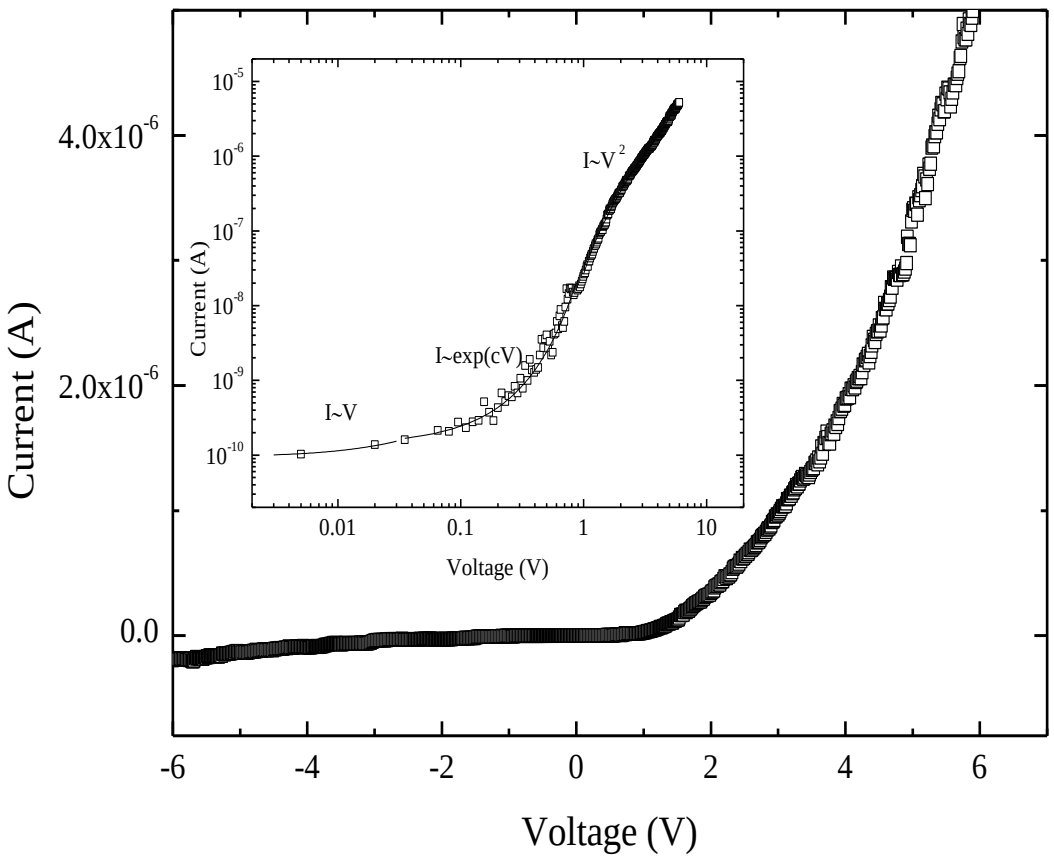
Current (A)
4.0x10-6
2.0x10-6
0.0
-6
-4
-2
0
2
4
6
Voltage (V)
Current (A)
10-5
10-6
10-7
10-8
10-9
10-10
0.01
0.1
1
10
Voltage (V)
I~V2
I~exp(cV)
I~V

Figure 3

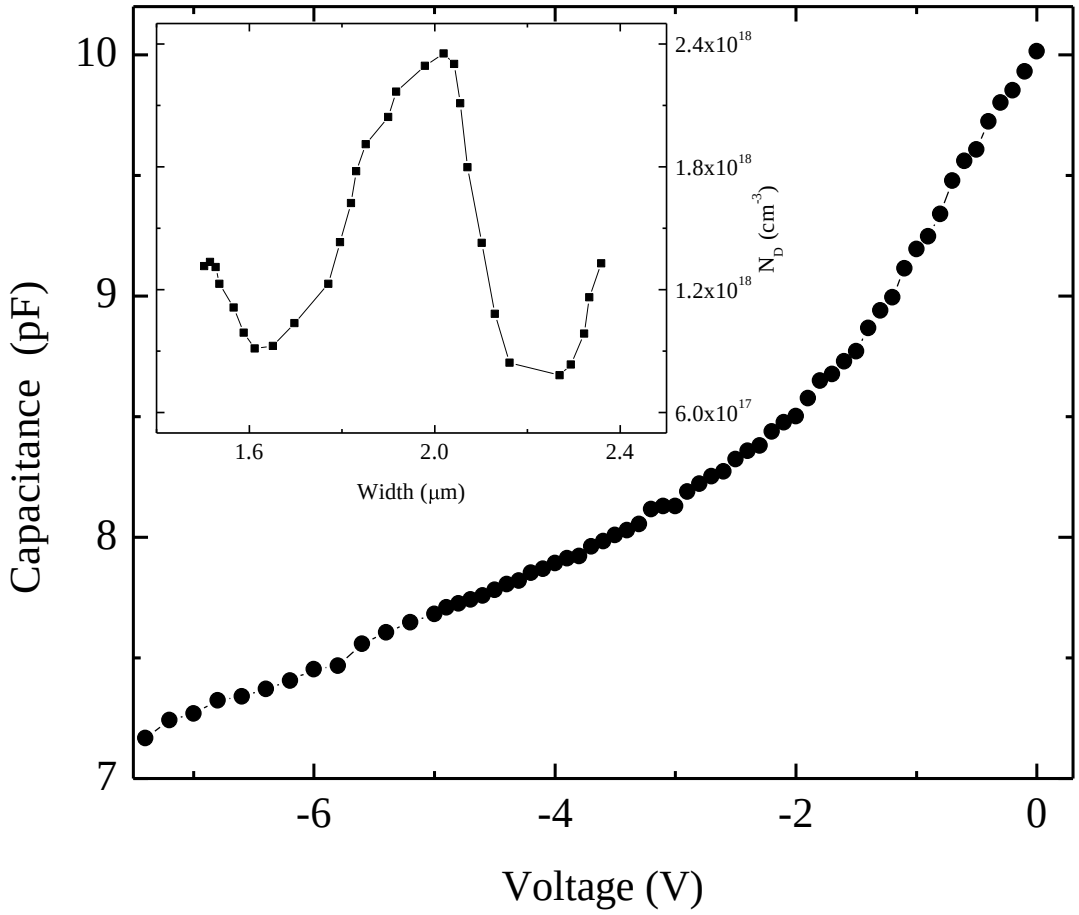
Capacitance (pF)
Voltage (V)
10
9
8
7
-6
-4
-2
0
2.4x10^18
1.8x10^18
1.2x10^18
6.0x10^17
N_D (cm^-3)
1.6
2.0
2.4
Width (μm)

Figure 4

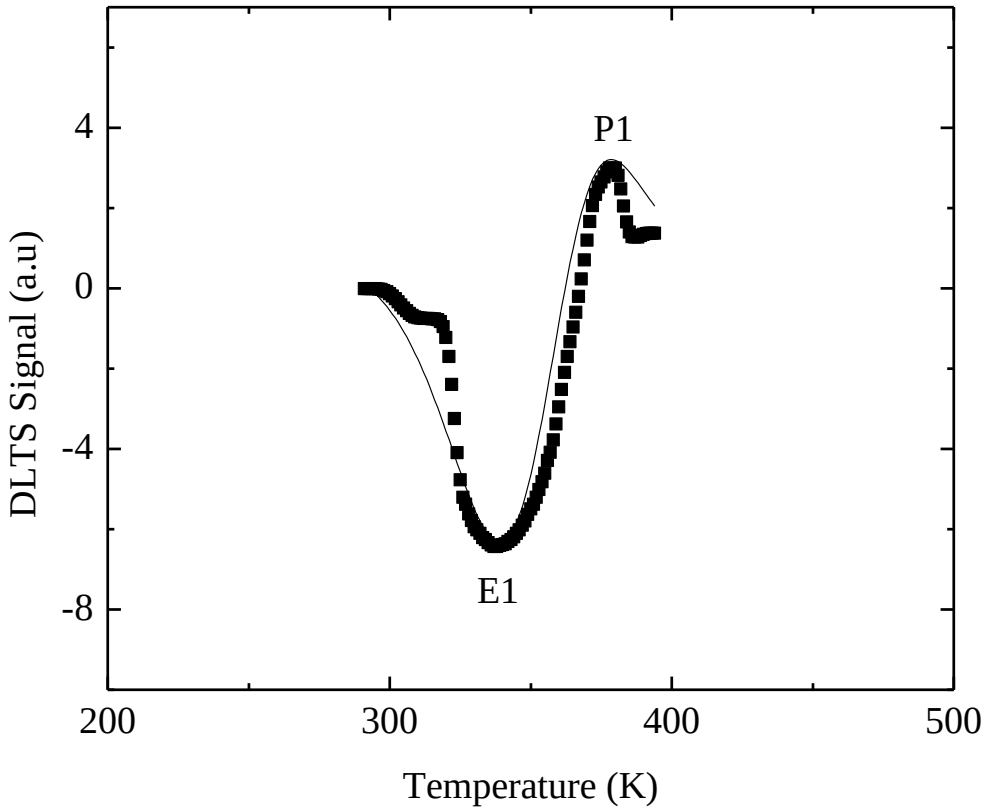

Figure 5 (a)

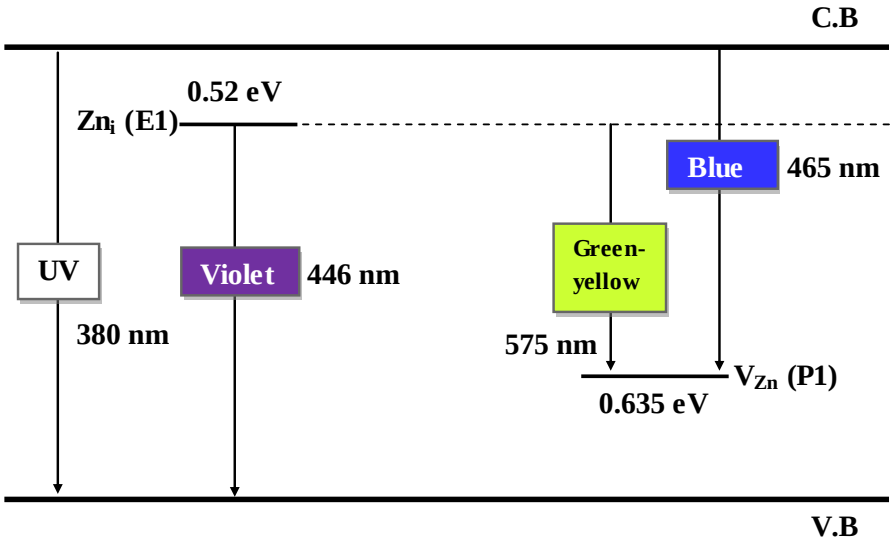

Figure 5 (b)

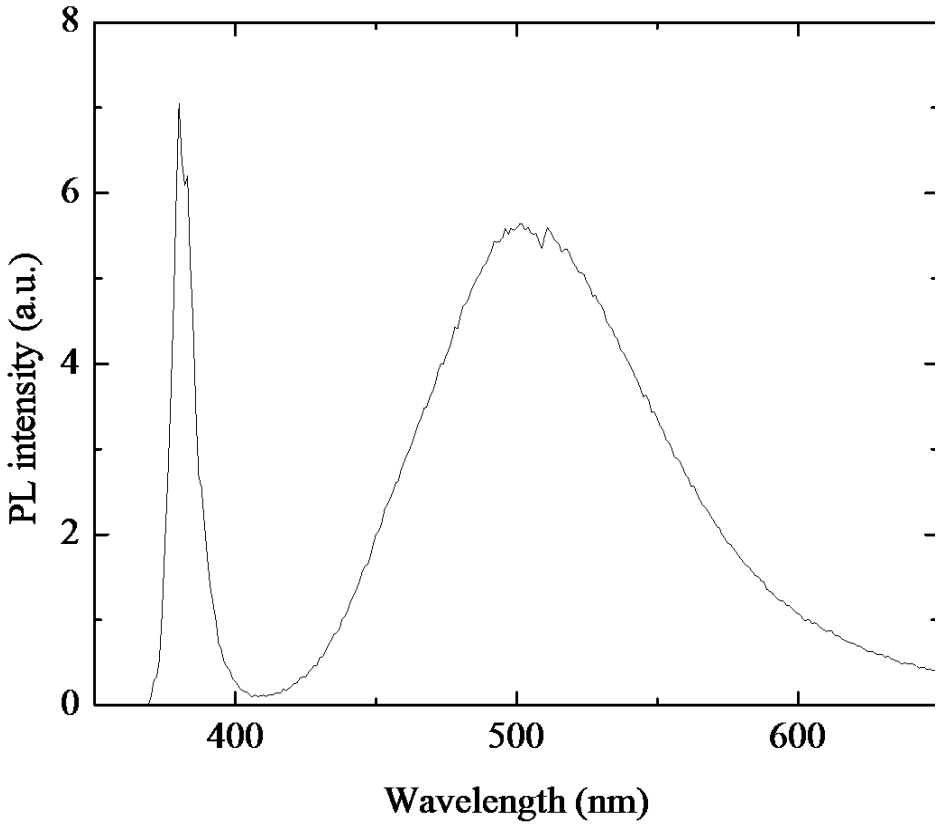

Figure 6